ADVANCED ENERGY MATERIALS
www.advenergymat.de

Unraveling the Fast Ionic Conduction in NASICON-Type Materials

Yufang He, Elena Scivally, Ajay Shaji, Bin Ouyang, and Yan Zeng**

Na Superionic Conductor (NASICON) materials stand out as an important class of ionic conductors, offering high ionic conductivity and notable electrochemical stability for applications such as solid electrolytes. While advances through compositional engineering have been made to enhance the ionic conductivity of NASICONs, the fundamental mechanisms underlying their superionic conducting behavior remain unresolved. In this study, the interplay between local and global factors—specifically, bottleneck volume and Na site ordering— that influence ionic conduction within the NASICON framework is elucidated. Analysis of reported ionic conductivity data indicates that optimal bottleneck volumes exceed 3.7 Å^3, adjustable through the choice of metal cations and polyanions. Additionally, the findings imply that weaker Na site ordering, which enhances ionic conduction, can be induced by increasing the Na content, selecting metal cations with a d^0 electron configuration, or mixing elements at the cation or polyanion sites. Moreover, it is proposed that the predominant diffusion mechanism can shift between occupancy-conserved hopping (OCH), occurring under conditions of strong Na site ordering, and single-ion hopping (SIH), which becomes possible when site ordering is minimal. These insights offer strategic guidelines for designing NASICONs with superionic conductivity, promoting the development of solid electrolytes for safer and more energy-dense all-solid-state batteries.

1. Introduction

The Na Superionic Conductor (NASICON) framework, identified in the 1970s,[1] has been widely studied and applied as solid electrolytes for all-solid-state batteries (ASSBs) attributed to its fast ion conduction, and robust thermal, chemical, and electrochemical stability. The NASICON framework has enabled the fast ion transport of alkali (Li or Na)[2–6] and alkaline earth metals (Mg or Ca).[7–11] The compositional flexibility of the NASICON framework allows for targeted optimization of its properties. The quest to optimize the ionic conductivity of various NASICONs has led to broad efforts in exploring the factors and mechanisms governing their fast ion transport.[3,4,12–15]

For Na-based NASICONs, ionic conductivities are typically enhanced through one or a combination of the multiple approaches: changing crystal structure, increasing Na content,[1,4,15,16] mixing $(SiO_4)^{4-}$ and $(PO_4)^{3-}$ polyanions,[1,4,15] doping with metals,[12,15,17,18] introducing lattice distortion,[19] optimizing bottleneck size,[1,20–24] or promoting "concerted" motion.[5,25,26] Some trends are well recognized: the rhombohedral phase with space group in $R\bar{3}c$ is usually more conductive than the monoclinic $C2/c$ phase due to more disordered Na occupancy in the former,[4,27] the optimal Na content ranges between 3.0 and 3.5 Na per formula unit,[3,15,28] introducing lattice distortion within a certain threshold is beneficial, and there is an optimal bottleneck size.[1,13,15,23,24] However, mixing polyanions or cations does not always lead to higher ionic conductivity.[15] In addition, the circumstances under which the "concerted" motion[5,26] occurs within the NASICON framework are not fully understood.

To untangle these complexities, we employ a synergistic approach that combines first-principles density functional theory (DFT) calculations with experimental validations to uncover the fundamental mechanisms that dictate the fast ionic conduction in NASICONs. This study focuses on the rhombohedral $R\bar{3}c$ phase due to its generally higher conductivities compared to the monoclinic $C2/c$ phase. Both phases have a similar framework, so it is expected that design principles for enhancing ionic conductivity could be transferable. We identify that all the known strategies for enhancing ion transport in NASICONs ultimately revolve around modulating two factors: the bottleneck size acts as a local factor that mediates the transition state of Na ions moving between sites, and the Na site ordering serves as a global factor that shapes the overall energy landscape of ion diffusion. Moreover, we identify occupancy conservation of low-energy Na sites as the fundamental origin for the enhanced ion transport through concerted motion that was proposed in previous studies.[26] We provide insights culminating in a precise strategy to optimize ionic conductivity by creating alkali (or alkaline earth) metal disordering while maintaining an adequate bottleneck size in the NASICON framework.

Y. He, E. Scivally, A. Shaji, B. Ouyang, Y. Zeng
Department of Chemistry and Biochemistry
Florida State University
Tallahassee, FL 32304, USA
E-mail: bouyang@fsu.edu; zeng@chem.fsu.edu

The ORCID identification number(s) for the author(s) of this article can be found under https://doi.org/10.1002/aenm.202403877

DOI: 10.1002/aenm.202403877

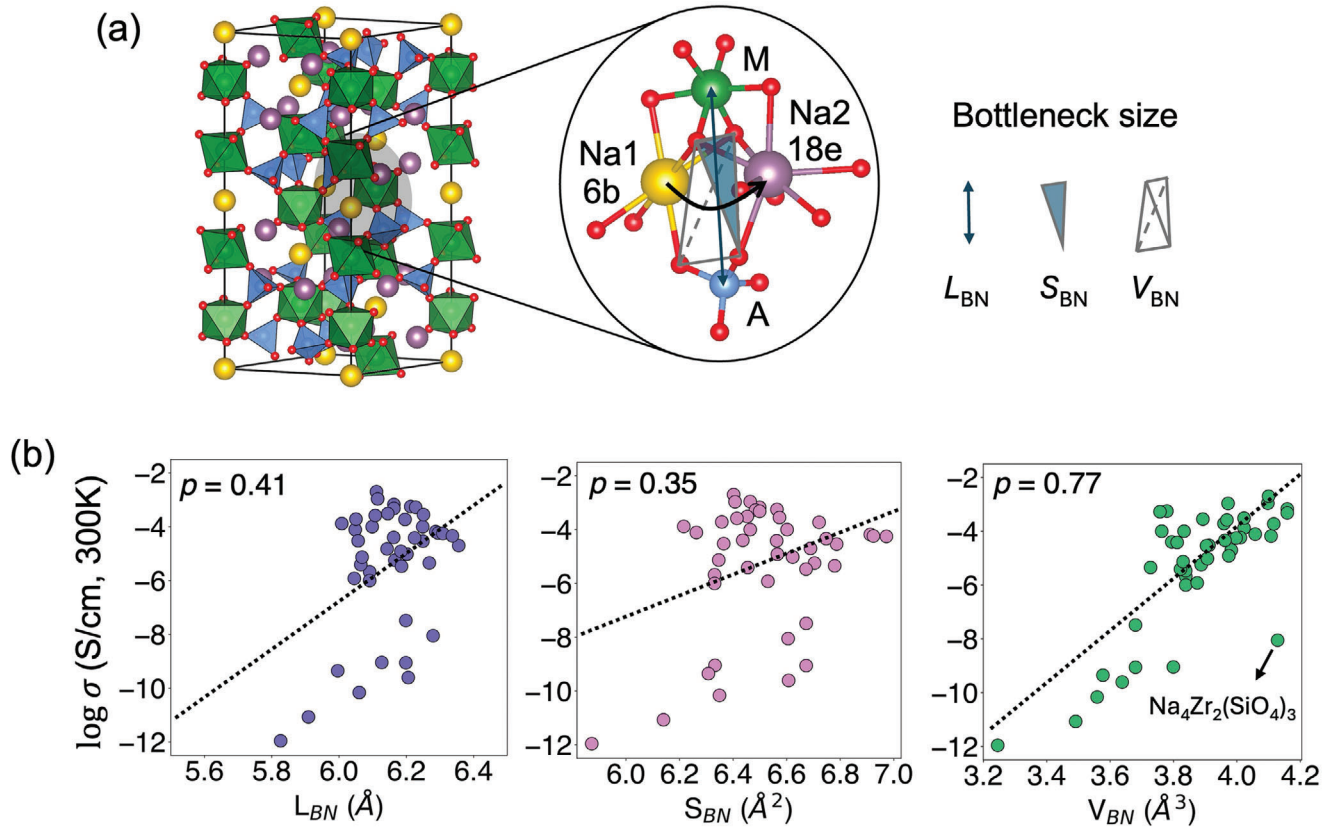

Figure 1. Bottleneck size and its effect on ionic conductivities in NASICONs. a) Schematic of the crystal structure of NASICON, with formula $Na_xM_2(AO_4)_3$, in rhombohedral $R\bar{3}c$ symmetry. M is a metal, (AO_4) is a polyanion. Na1 occupies a 6b site, while Na2 occupies a 18e site. Three ways to measure bottleneck size are shown: L_{BN} (bottleneck height), S_{BN} (bottleneck area), and V_{BN} (bottleneck volume). b) Correlation between ionic conductivity and L_{BN}, S_{BN}, and V_{BN}, respectively. The Pearson correlation (p) value is shown in each plot. The ionic conductivities and composition data of 46 NASICONs were extracted from the literature (Table S1, Supporting Information). $Na_4Zr_2(SiO_4)_3$[39] is pointed out as an outlier in the correlation between ionic conductivity and V_{BN}.

2. Results

2.1. Bottleneck Size as a Local Factor Dictating Ionic Conductivity

Na-NASICON is represented by a general chemical formula $Na_xM_2(AO_4)_3$, where the content of Na, x, depends on the total charge of the metal cations, M, and the polyanion, (AO_4). **Figure** 1a presents the most common crystal structure for Na-NASICON, rhombohedral with space group $R\bar{3}c$. The bottleneck site in $R\bar{3}c$ Na-NASICON is the distorted tetrahedral site (Wyckoff position 36f) that shares faces with the two neighboring sites, 6b and 18e, that Na normally occupies. Bottleneck size in NASICON structures is widely recognized as a critical determinant of Na ionic conductivity. Bottleneck size can be represented in three ways (Figure 1a): the height (L_{BN}) between the metal cation site (M) and the polyanion center (AO_4) that edge-shared with the bottleneck site, the area (S_{BN}) of the triangular cross-section passed by Na ions, and the volume (V_{BN}) of the bottleneck tetrahedron.[15,29–34] It has been ambiguous in the literature about which measure of bottleneck size (height, area, or volume) is the most critical one in determining the Na ionic conductivity in NASICONs.

We investigated the correlation of Na ionic conductivities in NASICONs with each of the three ways to quantify the bottleneck size. We employed text mining techniques to search for literature that reports ionic conductivities of Na-NASICONs, details described in previous work.[3,15,35–37] From the collected literature, we then manually curated the bulk ionic conductivities at 300 K from text, tables, a figures. When the ionic conductivities at 300 K are not directly reported in the literature, we calculated the values using the reported high-temperature conductivities and activation barriers by applying the Arrhenius relationship, $\sigma_T = A\exp(-\frac{E_a}{k_B T})$. Table S1 (Supporting Information) lists the compositions and bulk ionic conductivities of the 46 NASICONs, all in the rhombohedral phase.

The bottleneck sizes were analyzed from the corresponding structures relaxed in DFT.[3,15] Figure 1b plots the correlations between ionic conductivities and L_{BN}, S_{BN}, and V_{BN}, respectively. In all three cases, there is a minimum bottleneck size, approximately, $L_{BN} > 6.0$ Å, $S_{BN} > 6.2$ Å^2, and $V_{BN} > 3.7$ Å^3, for achieving ionic conductivities exceeding 10^{-4} S cm^{-1}. Pearson correlation coefficient (p)[38] for each plot is assessed and shown in Figure 1b. A $|p|$ value closer to 1 means a more linear correlation. We can see

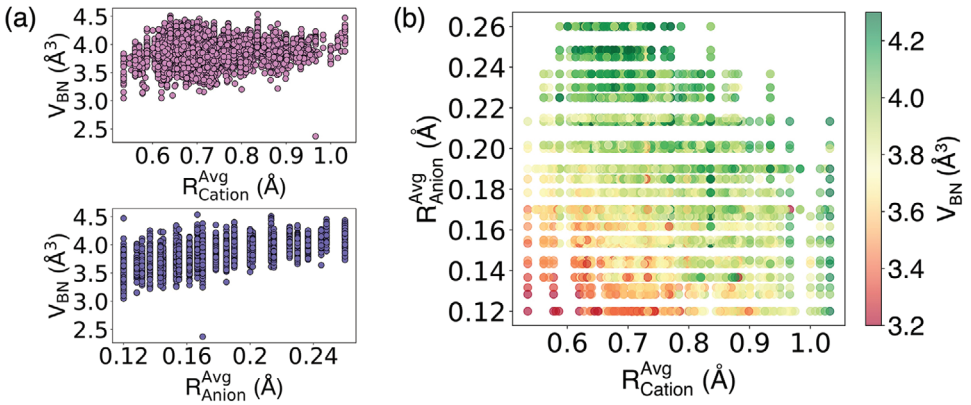

Figure 2. a) Correlation of bottleneck volume (V_{BN}) with an average cation radius (R^{Avg}_{Cation}) (upper panel) or average anion radius (R^{Avg}_{Anion}) (lower panel). b) 2D correlation of V_{BN} with R^{Avg}_{Cation} and R^{Avg}_{Anion}. A combination of a larger cation and a larger anion generally leads to a larger bottleneck volume.

that the bottleneck volume, V_{BN}, correlates the most linearly with ionic conductivity, with the highest p value of 0.77, compared to L_{BN} ($p = 0.41$) and S_{BN} ($p = 0.35$).

The bottleneck size in a NASICON is dependent on its chemical composition. We calculated the bottleneck volumes (V_{BN}) of 3881 NASICONs with distinct compositions in the rhombohedral $R\bar{3}c$ structure, computed by DFT and reported in our previous work.[3] All the atomic structures can be found at the open-access website–the Materials Project.[40] **Figure 2a** shows the correlation between bottleneck volume (V_{BN}) and the average cation radius (R^{Avg}_{Cation}) or the average anion radius (R^{Avg}_{Anion}). In general, larger cations or anions lead to larger bottleneck volume. However, at the same cation or anion radius, the bottleneck volume can vary significantly. This means that changing R^{Avg}_{Cation} or R^{Avg}_{Anion} alone may not be effective enough on tuning bottleneck size hence the ionic conductivity. Figure 2b shows the correlation between V_{BN} with both R^{Avg}_{Cation} and R^{Avg}_{Anion}. We see that the threshold of favored V_{BN} (>3.7 Å^3) is achieved at the upper right region of the plot, meaning that it is these two radii together that govern the bottleneck size. We further assessed how Na content influences V_{BN}. As shown in Figure S1 (Supporting Information), there appears to be no obvious correlation between Na content and the average V_{BN} of NASICONs.

2.2. Site Ordering as a Global Factor Dictating Ionic Conductivity

In the correlation plot between ionic conductivity and bottleneck volume (Figure 1b), one outlier, $Na_4Zr_2(SiO_4)_3$, is pointed out. $Na_4Zr_2(SiO_4)_3$ has a large bottleneck but low ionic conductivity. This suggests that there exist other factors that influence the ionic conductivity of NASICONs. We suspect that the Na site ordering is one of the critical factors. **Figure 3a** illustrates the energy landscape for Na ion diffusion in NASICON with ordered Na sites, where 6b is the lower-energy site compared to 18e which Na can occupy. The site energy difference between 6b and 18e, $E^{Diff}_{6b\to18e}$, dictates the ordering tendencies of Na. The larger the energy difference between the two sites, the stronger the ordering on the lower-energy site. The activation barrier for Na migration from the 6b site to its nearest neighboring 18e site is comprised of two parts: the kinetically resolved activation (KRA) barrier, E^{KRA}_a, and half of the site energy difference, $E^{Diff}_{6b\to18e}/2$. Hence, a large site energy difference contributes to a high activation barrier for Na to move. As shown in Figure 3b, the calculated $E^{Diff}_{6b\to18e}$ of $NaM_2(PO_4)_3$ varies with different metal M (M = Ge, Ti, Sn, Zr, Hf). These results indicate that the choice of metal cations

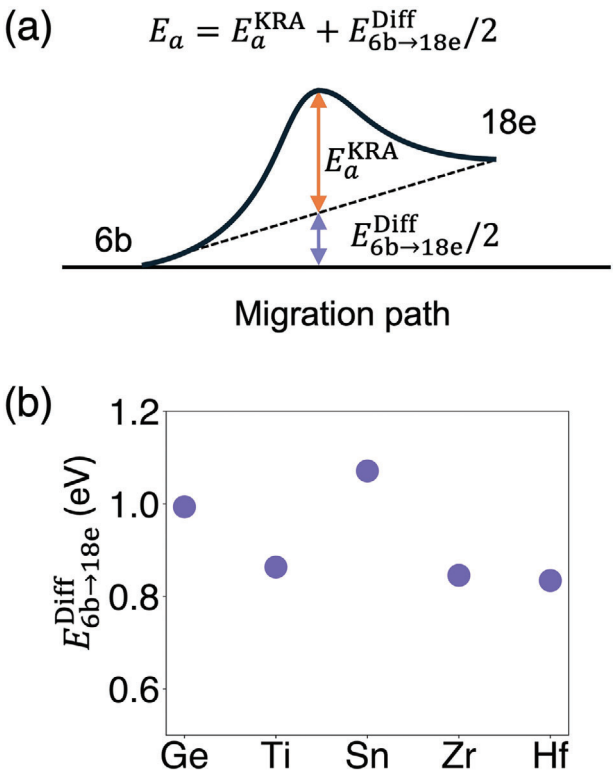

Figure 3. a) Schematic of the activation barrier (E_a) for Na migration from 6b to 18e site. E_a is composed of two parts: the kinetically resolved activation energy (E^{KRA}_a) and half of the site energy difference, $E^{Diff}_{6b\to18e}/2$. b) Calculated site energy difference between 6b and 18e sites in $NaM_2(PO_4)_3$ (M = Ge, Ti, Sn, Zr, Hf).

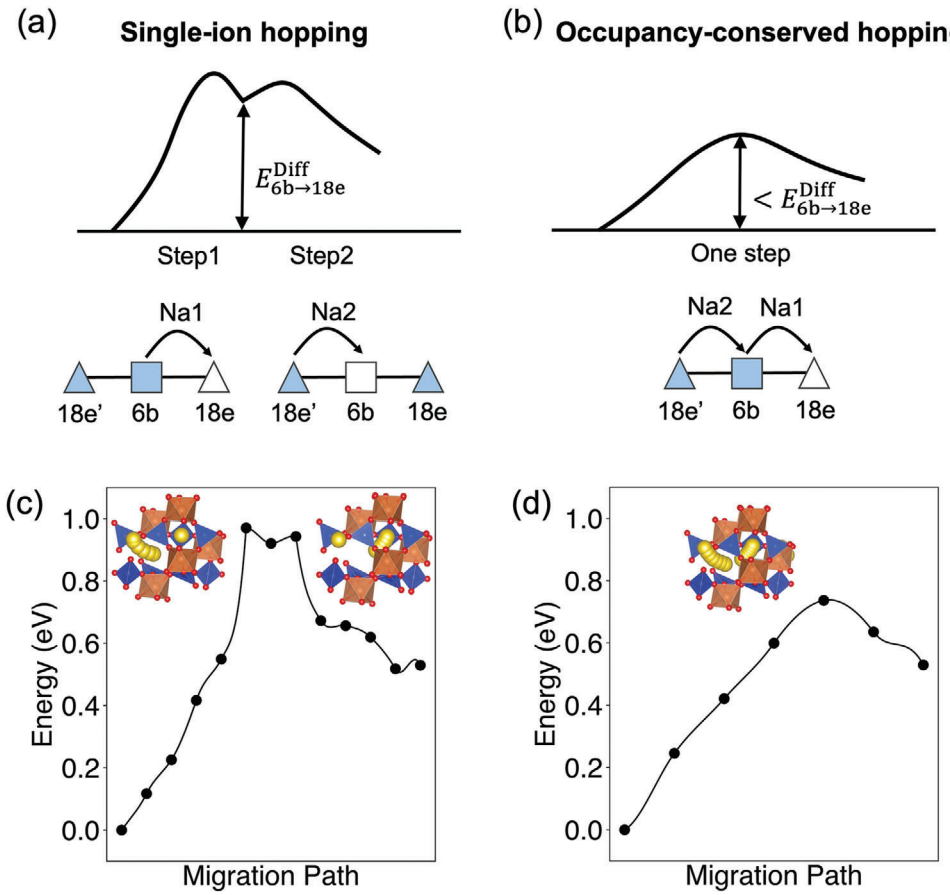

Figure 4. Ion diffusion mechanisms and the corresponding energy landscape in NASICONs. a) Schematic of the single-ion hopping (SIH) mechanism, which contains two steps: In step 1, Na1 hops from the 6b site to the 18e site, followed up by step 2, where Na2 hops from the 18e' site to the 6b site. b) Schematic of the occupancy-conserved hopping (OCH) mechanism, which contains one step: Immediately after Na1 departed from 6b, Na2 hops from 18e' to the 6b site to conserve 6b site occupancy of Na. c) Calculated energy landscape of Na diffusion in $Na_2Sb_2(SiO_4)_3$ following the SIH mechanism. d) Calculated energy landscape of Na diffusion in $Na_2Sb_2(SiO_4)_3$ under the OCH mechanism.

effectively influences the site energy difference between 6b and 18e. All these NASICON compounds exhibit $E_{6b\to18e}^{Diff}$ higher than 0.8 eV, indicating Na has a strong tendency to be ordered on the 6b site, and the activation barriers for Na diffusion are large. This can explain the low Na-ion conductivities of these materials observed in experiments.[1,41–46]

2.3. Diffusion Mechanism Governed by Site Ordering

To further identify the fundamental role played by the site ordering of Na in dictating its ionic conductivity, we need to understand the ion diffusion mechanism. We propose and examine two possible diffusion mechanisms in NASICONs: single-ion hopping (SIH) and occupancy-conserved hopping (OCH). In an ordered NASICON, the 6b site is usually energetically more favorable than the 18e site for Na to occupy, with an energy difference $E_{6b\to18e}^{Diff}$. The SIH process (**Figure 4a**) involves two steps of sequential hopping: Step 1, one Na (Na1) hops from a 6b site to an adjacent 18e site, overcoming an activation barrier primarily contributed by $E_{6b\to18e}^{Diff}$. Subsequently, in Step 2, another Na (Na2) hops from the 18e' site to the vacated 6b site. Figure 4c shows the energy landscape of the Na ion migration process through the SIH mechanism in a $R\bar{3}c$ $Na_2Sb_2(PO_4)_3$ calculated by the climbing image nudged elastic band (CI-NEB) theory. In $Na_2Sb_2(PO_4)_3$, the activation barrier for Na1 hopping from 6b to the neighboring 18e site is computed to be 0.921 eV. The following Na2 hopping from the 18e to 6b site leads to a downhill evolution in the energy landscape.

Conversely, the OCH mechanism, shown in Figure 4b, conserves 6b site occupancy of Na throughout the diffusion process. Under this mechanism, the Na1 hopping from 6b to 18e is immediately followed by Na2 hopping from a neighboring 18e' to the original 6b site where Na1 just departed. Note that in the OCH mechanism, the correlated hopping does not necessarily lead to simultaneous Na movement. We regard this occupancy conservation as the origin of the lower barrier created by concerted hopping as proposed by He et al.,[25] We hypothesize that the occupancy conservation in the OCH process is the key that contributes to a lower energy barrier because the lower-energy 6b site is never fully vacated during this process. Whenever one Na is about to leave the 6b site, there will be another Na getting ready to occupy this site. Consequently, the activation barrier of

the OCH process is expected to be lower than that of the SIH process.

To assess the energy landscape associated with the OCH process, we also used $R\bar{3}c$ $Na_2Sb_2(PO_4)_3$ as a model system. We moved Na1 and Na2 simultaneously during the NEB optimization steps so that the occupancy of the Na site can be conserved between the initial and the final states. In this case, the activation barrier of Na migration in $Na_2Sb_2(PO_4)_3$ via the OCH mechanism is computed to be 0.737 eV (Figure 4d), which is 0.184 eV lower than the case of SIH. This result supports our hypothesis that OCH leads to lower barriers due to site occupancy conservation. More importantly, it infers that the OCH process could be a more favorable diffusion mechanism of Na moving in NASICONs, especially when there is a strong ordering tendency.

2.4. Compositional Handles on Tuning Site Ordering and Ionic Conductivity

The site ordering of Na can significantly influence its transport in the NASICON framework, which in turn is controlled by the compositions. We investigated the effects of three compositional variables – Na content, d-shell electron configuration of the metal cation, and mixing on cation or anion site, respectively – on tuning the Na site ordering and ionic conductivity. The site energy difference, $E^{Diff}_{6b\rightarrow 18e}$, is applied as the metric of ordering tendency between 6b and 18e sites.

To assess the effect of Na content, we compare $NaZr_2(PO_4)_3$ and $Na_3Sc_2(PO_4)_3$, which have similar bottleneck sizes and similar cations (Sc^{3+} and Zr^{4+} are d^0 species with ionic radius of 0.745 and 0.72 Å, respectively). **Figure** 5a depicts the energy landscape associated with Na migration from 6b to 18e sites in $NaZr_2(PO_4)_3$ and $Na_3Sc_2(PO_4)_3$. The energy difference between the starting and ending points in each plot represents the site energy difference between 6b and 18e, $E^{Diff}_{6b\rightarrow 18e}$. As we can see, $Na_3Sc_2(PO_4)_3$ presents a negligible $E^{Diff}_{6b\rightarrow 18e}$ and much lower activation energy compared to $NaZr_2(PO_4)_3$. This result indicates that Na content can effectively tune the ordering tendency of Na.

To assess the effect of electron configuration (d^0 versus d^{10}) of metal cations, we calculated the energy evolution of Na migrating from 6b to 18e sites in $Na_3In_2(PO_4)_3$ and $Na_3Sc_2(PO_4)_3$. As shown in Figure 5b, the activation energy of $Na_3Sc_2(PO_4)_3$ is significantly lower than that of $Na_3In_2(PO_4)_3$. This lower site energy difference between 6b and 18e in $Na_3Sc_2(PO_4)_3$ suggests a weaker ordering tendency compared to $Na_3In_2(PO_4)$. Notably, Sc^{3+} has a smaller ionic radius (0.745 Å) than In^{3+} (0.8 Å), indicating that the bottleneck size does not dominate the influence on ionic conductivity in this case. Rather, Sc^{3+} in $Na_3Sc_2(PO_4)_3$ has a d^0 electron configuration with an empty 3d subshell, whereas In^{3+} in $Na_3In_2(PO_4)_3$ has a d^{10} electron configuration with a fully filled 4d subshell. Previous studies have revealed that the electronic structure of transition metals can influence their tolerance of bond distortion, thereby governing the stability of materials.[28,47] Here we reveal that the electronic structure also affects the energy landscape of ion diffusion, as ion migration is always accompanied by bond distortion.

We further assessed the correlation between the structural stability (represented as energy above the hull, E_{hull}) and bond length deviation of metal-oxygen (M—O) bonds in 3881 calculated NASICONs.[3] Figure S2a (Supporting Information) shows that NASICONs with d^0 metal cations do not have a clear correlation between M—O bond deviation and structural stability. In contrast, NASICONs with d^{10} metal cations become less stable as M—O bond deviation increases (Figure S2b, Supporting Information). This analysis indicates that metal cations with d^0 electron configuration in NASICONs could tolerate larger M—O bond distortions. Consequently, the energy landscape in NASICONs containing d^0 metal cations could be more flattened, as the bond distortion fluctuations during ion migration have a much less pronounced impact on energy.

We also evaluated the influence of elemental mixing on the cation or polyanion site on Na ordering and ionic conductivity. Figure 5c shows that by introducing cation or polyanion mixing to the base compound $NaZr_2(PO_4)_3$, using $NaHfZr(PO_4)_3$, $NaNbIn(PO_4)_3$ and $NaZr_2(SO_4)_{1.5}(SiO_4)_{1.5}$ as three examples, the site energy difference and the activation barrier can be lowered. The selection of these three compounds represents three ways of mixing: $NaHfZr(PO_4)_3$ representing mixing cations with the same valence state, $NaNbIn(PO_4)_3$ representing mixing cations with different valence states, and $NaZr_2(SO_4)_{1.5}(SiO_4)_{1.5}$ representing mixing different polyanions. It is shown in Figure 5c that all three types of ion mixing can lead to lower site energy differences between 6b and 18e sites, thus implying the effectiveness of mixing ions for enhancing ionic conductivity by promoting site disordering, particularly when there is a strong ordering tendency.

To validate the calculation results, we synthesized $Na_3Sc_2(PO_4)_3$, $Na_3In_2(PO_4)_3$, and $NaNbIn(PO_4)_3$ by solid-state reaction and measured their Na-ion conductivities using electrochemical impedance spectroscopy. $NaZr_2(PO_4)_3$ was made and evaluated in our previous work using the same procedure.[28] X-ray diffraction (XRD) patterns and structural refinements of $Na_3Sc_2(PO_4)_3$, $Na_3In_2(PO_4)_3$, and $NaNbIn(PO_4)_3$ are shown in Figure S3 (Supporting Information). These three compounds are found to be a pure phase in rhombohedral $R\bar{3}c$, the same structure as the reported $NaZr_2(PO_4)_3$. Figure 5d shows the Nyquist plots of $NaZr_2(PO_4)_3$, $Na_3Sc_2(PO_4)_3$, $Na_3In_2(PO_4)_3$, and $NaNbIn(PO_4)_3$ obtained at room temperature. The total Na-ion conductivities of $NaZr_2(PO_4)_3$, $Na_3Sc_2(PO_4)_3$, $Na_3In_2(PO_4)_3$, and $NaNbIn(PO_4)_3$ are 3.5×10^{-7}, 9.2×10^{-5}, 1.8×10^{-5}, and 1.1×10^{-6} S cm^{-1} respectively (Figure 5e; Table S2, Supporting Information). Comparison of the measured ionic conductivities agrees with the calculated migration energy, confirming that by increasing Na content, using d^0 metals, or applying cation or polyanion mixing, less ordered Na site and higher ionic conductivity could be achieved. It is also reported that the ionic conductivity of $Na_3Hf_{1.5}Mg_{0.5}(SiO_4)(PO_4)_2$ is higher than $Na_3HfMg(PO_4)_3$ even with very close cation radius between Hf^{4+} (0.71 Å) and Mg^{2+} (0.72 Å), which supports that polyanion mixing of NASICON can increase its ionic conductivity.[15]

3. Discussion

Previous discussions in the literature have suggested concerted motion, or more precisely, occupancy-conserved hopping (OCH), as the underlying mechanism leading to high ionic conductivity

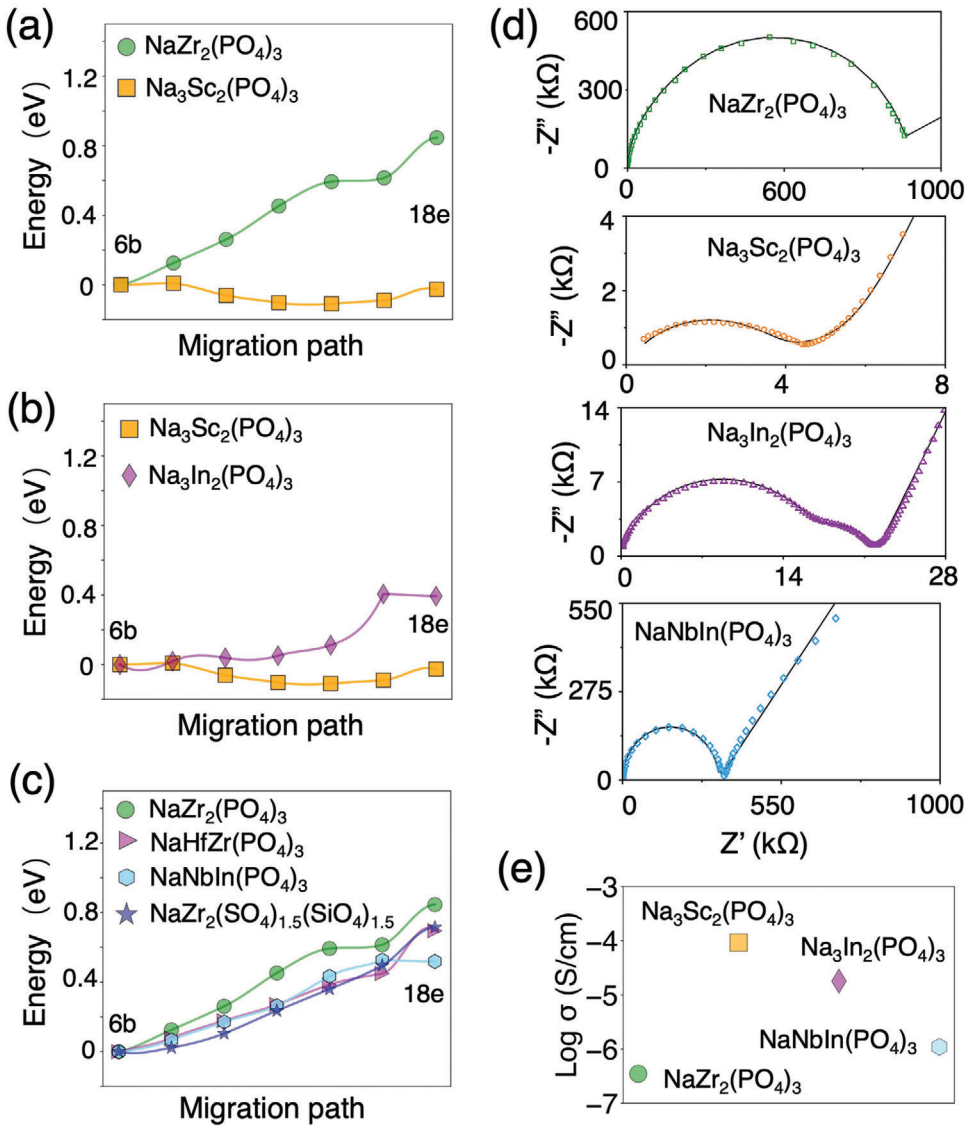

Figure 5. Energy landscape and ionic conductivities mediated by Na content, d^0 vs d^{10} metal cations, and elemental mixing on cation or polyanion site. Energy evolution along the migration path from 6b to 18e site in a) $NaZr_2(PO_4)_3$ and $Na_3Sc_2(PO_4)_3$, b) $Na_3Sc_2(PO_4)_3$ and $Na_3In_2(PO_4)_3$, and c) $NaZr_2(PO_4)_3$, $NaHfZr(PO_4)_3$, $NaNbIn(PO_4)_3$, and $NaZr_2(SO_4)_{1.5}(SiO_4)_{1.5}$. d) Nyquist plots obtained from room temperature impedance measurements on pellets made from $NaZr_2(PO_4)_3$, $Na_3Sc_2(PO_4)_3$, $Na_3In_2(PO_4)_3$, and $NaNbIn(PO_4)_3$. Open symbols represent measured data and solid lines represent fitting results. e) The corresponding ionic conductivities of $NaZr_2(PO_4)_3$ $Na_3Sc_2(PO_4)_3$, $Na_3In_2(PO_4)_3$, and $NaNbIn(PO_4)_3$.

in crystalline frameworks including NASICON.[5,24,25] We found that when there is a strong ordering tendency of the charge carrier ions (e.g., Na, Li, Ca, Mg), OCH mechanism is indeed an effective way to reduce the activation barrier by reducing the occupancy perturbation during ion migration, as demonstrated in the case of $Na_2Sb_2(SiO_4)_3$ (Figure 4d). However, when there is minimal ordering tendency, OCH is not necessarily the favored mechanism. **Figure** 6a compares the two diffusion mechanisms (SIH vs OCH) applied to $Na_3Sc_2(PO_4)_3$, where 6b and 18e sites have negligible energy differences. It is shown that the two mechanisms lead to similar activation barriers, suggesting that either mechanism could occur. Figure 6b shows the calculated energy landscape of $Na_3HfMg(PO_4)_3$, which is also associated with a smaller energy difference between 6b and 18e sites. In this case, the SIH is even more favorable with a lower activation barrier than OCH.

We attribute the origin of high conductivity in NASICONs to an interplay between bottleneck size and site ordering. The bottleneck size determines the coordination environment at the saddle point and hence the kinetically resolved barrier. Meanwhile, site energy difference controls the energy fluctuation upon the change in site occupancy change during ion migration. To design NASICONs with high ionic conductivity, one should first design a compound with an optimized bottleneck volume (greater than 3.7 $Å^3$), which can be achieved by using sufficiently large cations and polyanions. In addition to having an optimal bottleneck size, it is also important to flatten the energy landscape of the charge-carrier ion by minimizing its site energy difference hence to

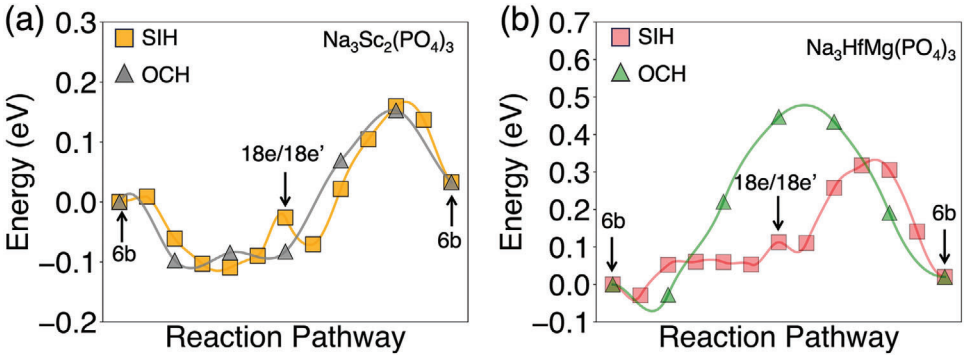

Figure 6. Computed energy landscape for two diffusion mechanisms, single-ion hopping (SIH) and oocupancy-conserved hopping (OCH) in a) $Na_3Sc_2(PO_4)_3$ and b) $Na_3HfMg(PO_4)_3$.

reduce site ordering tendency, which can be achieved by increasing the Na content, using d^0 metal cations, or introducing cations or anion mixing. Although this work focuses on NASICONs in rhombohedral $R\bar{3}c$ phase, the conclusions should be applicable to another NASICON phase–monoclinic with $C2/c$ space group. The monoclinic phase has the same framework as the rhombohedral NASICONs while having more ordered Na occupancies.[4,26] It is also worth mentioning that compounds with mixed cations or polyanions might be challenged by synthetic accessibility, as shown in previous computational predictions.[15] Therefore, novel synthesis routes for NASICONs with compositional disorder will be beneficial for developing NASICON compounds with fast ionic conduction.[48]

4. Experimental Section

Synthesis and Characterization: Solid-state reaction was employed for the synthesis of $NaNbIn(PO_4)_3$, $Na_3Sc_2(PO_4)_3$, and $Na_3In_2(PO_4)_3$. The source of Na was provided by Na_2CO_3, and it was used 10 wt.% in excess to account for the Na loss during elevated annealing temperatures. Commercially available metal oxides (Nb_2O_5, In_2O_3, Sc_2O_3) were used as precursors for integrating the metal cations. $NH_4H_2PO_4$ was used to provide PO_4. Synthesis was carried out by mixing the required precursors into a slurry using ethanol in a planetary ball mill at 250 rpm for 12 h. The slurry was later dried and preheated for 12 h (at 300 °C). After preheating, the obtained solids were pulverized using a mortar and pestle, pelletized, and heated at 1100 °C for 12 h. Each of the samples was air-quenched at the end of the designated time. Fast-cooled pellets were ground to powder for further characterization and analysis.

Rigaku Miniflex 600 diffractometer with Cu Kα radiation was used to obtain the crystal structures of the three compounds. Rietveld refinements against X-ray diffraction patterns were obtained using the GSAS-II software. VESTA software was used for the visualization of the atomic structures.

Conductivity Measurement: Biologic VPM-300 potentiostat was employed for the measurement of ionic conductivities of the three compounds. As synthesized powders were crushed in a 50 mL zirconia jar using a SPEX 800M mixer mill for 30 min. These powders were pelletized (6 mm diameter) and sintered at 1050 °C, followed by rapid cooling. The pellets were sandwiched between indium metal foils and pressed in a cold isotactic press to obtain good contact between the junctions. AC impedance measurements were performed at 23 °C (room temperature). The potentiostat frequency spans from a range of 7 MHz to 50 mHz with a 10 mV excitation voltage applied during the measurements. Ionic conductivity calculations were carried out by fitting the impedance spectra using the ZView software. Equivalent circuit representation contains R1-CPE1, R2-CPE-2, and CPE-3 connected in series, where R is the ohmic resistance and CPE stands for constant phase element. R1-CPE1 and R2-CPE2 are attributed to ion transport in bulk and grain boundaries, respectively. CPE3 represents the low-frequency diffusion in the equivalent circuit.

First-Principles Calculations: First-principles calculations were performed via the Vienna ab initio simulation package (VASP).[49,50] The Projector augmented-wave (PAW) potential was used for electron and core interactions and the Perdew–Burke–Ernzerhof (PBE) generalized gradient approximation (GGA) was employed to approximate the exchange-correlation function.[49–51] The electronic wave functions were expanded on a plane-wave basis set of 520 eV. In addition, a reciprocal space discretization of 25 k-points per/Å was applied, and the convergence criteria were set to 10^{-6} eV for electronic iterations and 0.02 eV $Å^{-1}$ for ionic iterations for all the structural optimizations and total energy calculations. The Climbing Image Nudged Elastic Band (CI-NEB) method was applied for the activation energy calculations. The site energy difference of NASICON when Na occupying 6b and 18e sites during Na ion migration was calculated by DFT as well.

Supporting Information

Supporting Information is available from the Wiley Online Library or from the author.

Acknowledgements

This work is supported by the startup funding for Profs. Zeng and Ouyang, respectively, from Florida State University. The Computational resources were provided by the Advanced Cyberinfrastructure Coordination Ecosystem: Services & Support (ACCESS), the National Energy Research Scientific Computing Center (NERSC), a DOE Office of Science User Facility supported by the Office of Science and the U.S. Department of Energy under contract no. DE-AC02- 05CH11231 and no. DE-LC-0000119, and Research Computing Center (RCC) at Florida State University. The computation and data processing were also supported by the supercomputing resources from the Department of Energy's Office of Energy Efficiency and Renewable Energy at the National Renewable Energy Laboratory.

Conflict of Interest

The authors declare no conflict of interest.

Data Availability Statement

The data that support the findings of this study are available in the supplementary material of this article.

Keywords

bottleneck size, ionic conductivity, NASICON, occupancy-conserved hopping (OCH), single-ion hopping (SIH), site ordering

Received: August 27, 2024
Published online:

[1] J. B. Goodenough, H. Y. P. Hong, J. A. Kafalas, *Mater. Res. Bull.* **1976**, *11*, 203.
[2] J.-M. Winand, A. Rulmont, P. Tarte, *J. Solid State Chem.* **1991**, *93*, 341.
[3] B. Ouyang, J. Wang, T. He, C. J. Bartel, H. Huo, Y. Wang, V. Lacivita, H. Kim, G. Ceder, *Nat. Commun.* **2021**, *12*, 5752.
[4] Z. Deng, G. Sai Gautam, S. K. Kolli, J. N. Chotard, A. K. Cheetham, C. Masquelier, P. Canepa, *Chem. Mater.* **2020**, *32*, 7908.
[5] Z. Zhang, Z. Zou, K. Kaup, R. Xiao, S. Shi, M. Avdeev, Y. S. Hu, D. Wang, B. He, H. Li, X. Huang, L. F. Nazar, L. Chen, *Adv. Energy Mater.* **2019**, *9*, 1902373.
[6] Q. Zhou, B. Xu, P. H. Chien, Y. Li, B. Huang, N. Wu, H. Xu, N. S. Grundish, Y. Y. Hu, J. B. Goodenough, *Small Methods* **2020**, *4*, 2000764.
[7] Z. Zhang, L. F. Nazar, *Nat. Rev. Mater.* **2022**, *7*, 389.
[8] L. E. Blanc, Y. Choi, A. Shyamsunder, B. Key, S. H. Lapidus, C. Li, L. Yin, X. Li, B. Gwalani, Y. Xiao, C. J. Bartel, G. Ceder, L. F. Nazar, *Chem. Mater.* **2023**, 468.
[9] D. B. Tekliye, A. Kumar, X. Weihang, T. D. Mercy, P. Canepa, G. Sai Gautam, *Chem. Mater.* **2022**, *34*, 10133.
[10] A. Chakraborty, R. Thirupathi, S. Bhattacharyya, K. Singh, S. Omar, *J. Power Sources* **2023**, *572*, 233092.
[11] C. E. Özbilgin, K. Kobayashi, S. Tamura, N. Imanaka, T. S. Suzuki, *Ceram. Int.* **2022**, *48*, 10733.
[12] F. Sun, Y. Xiang, Q. Sun, G. Zhong, M. N. Banis, Y. Liu, R. Li, R. Fu, M. Zheng, T. K. Sham, Y. Yang, X. Sun, X. Sun, *Adv. Funct. Mater.* **2021**, *31*, 2102129.
[13] N. Anantharamulu, K. Koteswara Rao, G. Rambabu, B. Vijaya Kumar, V. Radha, M. Vithal, *J. Mater. Sci.* **2011**, *46*, 2821.
[14] Y. B. Rao, K. K. Bharathi, L. N. Patro, *Solid State Ionics* **2021**, *366–367*, 115671.
[15] J. Wang, T. He, X. Yang, Z. Cai, Y. Wang, V. Lacivita, H. Kim, B. Ouyang, G. Ceder, *Nat. Commun.* **2023**, *14*, 5210.
[16] H. Aono, E. Suginoto, *J. Am. Ceram. Soc.* **1996**, *79*, 2786.
[17] E. A. Cheung, H. Nguyen, M. Avdeev, N. R. de Souza, Y. S. Meng, N. Sharma, *Chem. Mater.* **2021**, *33*, 8768.
[18] L. Ran, A. Baktash, M. Li, Y. Yin, B. Demir, T. Lin, M. Li, M. Rana, I. Gentle, L. Wang, D. J. Searles, R. Knibbe, *Energy Storage Mater.* **2021**, *40*, 282.
[19] Y. Zeng, B. Ouyang, J. Liu, Y. W. Byeon, Z. Cai, L. J. Miara, Y. Wang, G. Ceder, *Science* **2022**, *378*, 1320.
[20] M. Avdeev, *Chem. Mater.* **2021**, *33*, 7620.
[21] A. Martínez-Juárez, C. Pecharromán, J. E. Iglesias, J. M. Rojo, *J. Phys. Chem. B* **1998**, *102*, 372.
[22] L. Zhu, Y. Wang, J. Chen, W. Li, T. Wang, J. Wu, S. Han, Y. Xia, Y. Wu, M. Wu, F. Wang, Y. Zheng, L. Peng, J. Liu, L. Chen, W. Tang, *Sci. Adv.* *8*, eabj7698.
[23] Z. Zou, N. Ma, A. Wang, Y. Ran, T. Song, B. He, A. Ye, P. Mi, L. Zhang, H. Zhou, Y. Jiao, J. Liu, D. Wang, Y. Li, M. Avdeev, S. Shi, *Adv. Funct. Mater.* **2021**, *31*, 2107747.
[24] L. Zhang, Y. Liu, Y. You, A. Vinu, L. Mai, *Interdiscip. Mater.* **2023**, *2*, 91.
[25] Z. Zou, N. Ma, A. Wang, Y. Ran, T. Song, Y. Jiao, J. Liu, H. Zhou, W. Shi, B. He, D. Wang, Y. Li, M. Avdeev, S. Shi, *Adv. Energy Mater.* **2020**, *10*, 2001486.
[26] X. He, Y. Zhu, Y. Mo, *Nat. Commun.* **2017**, *8*, 15893.
[27] D. Morgan, G. Ceder, J. B., Saïdi,, J. Swoyer, H. Huang, G. Adamson, *Chem. Mater.* **2002**, *14*, 4684.
[28] Z. Deng, T. P. Mishra, E. Mahayoni, Q. Ma, A. J. K. Tieu, O. Guillon, J. N. Chotard, V. Seznec, A. K. Cheetham, C. Masquelier, G. S. Gautam, P. Canepa, *Nat. Commun.* **2022**, *13*, 4470.
[29] Z. Zou, N. Ma, A. Wang, Y. Ran, T. Song, B. He, A. Ye, P. Mi, L. Zhang, H. Zhou, *Adv. Funct. Mater.* **2021**, *31*, 2107747.
[30] H. Park, K. Jung, M. Nezafati, C. S. Kim, B. Kang, *ACS Appl. Mater. Interfaces* **2016**, *8*, 27814.
[31] S. Song, H. M. Duong, A. M. Korsunsky, N. Hu, L. Lu, *Sci. Rep.* **2016**, *6*, 32330.
[32] H. P. Hong, *Mater. Res. Bull.* **1976**, *11*, 173.
[33] M. Guin, F. Tietz, *J. Power Sources* **2015**, *273*, 1056.
[34] Z. Zou, N. Ma, A. Wang, Y. Ran, T. Song, Y. Jiao, J. Liu, H. Zhou, W. Shi, B. He, *Adv. Energy Mater.* **2020**, *10*, 2001486.
[35] E. R. Losilla, M. A. G. Aranda, S. Bruque, M. A. París, J. Sanz, A. R. West, *Chem. Mater.* **1998**, *10*, 665.
[36] Q. Ma, M. Guin, S. Naqash, C. L. Tsai, F. Tietz, O. Guillon, *Chem. Mater.* **2016**, *28*, 4821.
[37] E. R. Losilla, M. A. G. Aranda, S. Bruque, J. Sanz, M. A. París, J. Campo, A. R. West, *Chem. Mater.* **2000**, *12*, 2134.
[38] M. S. Stephen, *Stat. Sci.* **1989**, *4*, 73.
[39] D. T. Qui, J. J. Capponi, J. C. Joubert, R. D. Shannon, *J. Solid State Chem.* **1981**, *39*, 219.
[40] A. Jain, S. P. Ong, G. Hautier, W. Chen, W. D. Richards, S. Dacek, S. Cholia, D. Gunter, D. Skinner, G. Ceder, *APL Mater.* **2013**, *1*, 011002.
[41] M. P. Carrasco, M. C. Guillem, J. Alamo, *Solid State Ionics* **1993**, *63–65*, 684.
[42] H. Y. P. Hong, *Mater. Res. Bull.* **1976**, *11*, 173.
[43] W. J. Cui, J. Yi, L. Chen, C. X. Wang, Y. Y. Xia, *J. Power Sources* **2012**, *217*, 77.
[44] M. Illbeigi, A. Fazlali, M. Kazazi, A. H. Mohammadi, *Solid State Ionics* **2016**, *289*, 180.
[45] H. Rusdi, N. S. Mohamed, R. H. Y. Subban, R. Rusdi, *J. Sci.: Adv. Mater. Devices* **2020**, *5*, 368.
[46] A. Martínez-Juárez, J. E. Iglesias, J. Rojo, *Solid State Ionics* **1996**, *91*, 295.
[47] A. Urban, A. Abdellahi, S. Dacek, N. Artrith, G. Ceder, *Phys. Rev. Lett.* **2017**, *119*, 176402.
[48] B. Ouyang, Y. Zeng, *Nat. Commun.* **2024**, *15*, 973.
[49] G. Kresse, J. Furthmüller, *Phys Rev B Condens Matter* **1996**, *54*, 11169.
[50] J. P. Perdew, K. Burke, M. Ernzerhof, *Phys. Rev. Lett.* **1996**, *77*, 3865.
[51] G. Kresse, J. Furthmüller, *Comput. Mater. Sci.* **1996**, *6*, 15.